Open Veterinary Journal, (2025), Vol. 15(1): 325-338
ISSN: 2226-4485 (Print)
ISSN: 2218-6050 (Online)

Research Article
DOI: *10.5455/OVJ.2025.v15.i1.31*

Submitted: 01/12/2024 Accepted: 30/12/2024 Published: 31/01/2025

The impact of autogenous bone grafts on the regeneration of radial bone defects in rabbits compared to autogenous advanced platelet-rich fibrin plus

Taher N. Elmeshreghi[1]*, Fathy D. El-Seddawy[2], Mohamed Gomaa[2], Mustafa Abd El Raouf[2] and Shimaa A. Ezzeldein[2]

[1]*Department of Surgery and Theriogenology, Faculty of Veterinary Medicine, University of Tripoli, Tripoli, Libya*
[2]*Department of Surgery, Anesthesiology and Radiology, Faculty of Veterinary Medicine, Zagazig University, Zagazig, Egypt*

ABSTRACT

Background: Bone grafts are an established treatment performed for managing segmental bone defects resulting from tumors, infections, high-energy trauma, congenital deformities, and nonunion.

Aim: To determine the regenerative potential following the sole implantation of rib, coccygeal, and advanced platelet-rich fibrin plus (A-PRF+) autografts to repair radial bone defects in rabbits.

Methods: Radial mid-shaft defects of 10 mm were created on the left limb of 24 rabbits. The animals were randomly assigned to four groups based on the type of defect filling: control (no filler), A-PRF+, coccygeal, and rib. Diagnostic imaging modalities, including X-rays and computed tomography (CT), with macro- and micro-histopathological examinations, were employed for postoperative assessment at 6 weeks ($n = 3$) and 12 weeks ($n = 3$), respectively.

Results: The statistical analysis of quantitative bone formation scores of diagnostic imaging and histopathology at 6 weeks postoperatively demonstrated fundamental significance differences between the rib and control groups and the coccygeal and control groups ($p < 0.05$). The radiographic scoring method at 6 weeks indicated a statistically significant difference between the rib and A-PRF+ groups ($p < 0.01$), in addition to the coccygeal and A-PRF+ groups ($p < 0.01$). In the CT evaluation, a significant difference was observed between the rib and A-PRF+ groups ($p < 0.05$). All A-PRF+ quantitatively assessed methods exhibited no statistically significant difference between the A-PRF+ and control groups at 6 weeks postoperatively. At 12 weeks, the A-PRF+, coccygeal, and rib groups presented substantial differences from the control group as evidenced by X-rays, CT scans, and macro- and micro-histopathological analyses.

Conclusion: The implantation of autograft rib and coccygeal bone to treat radial bone defects proved a significantly enhanced capacity for promoting bone ingrowth. In addition, coccygeal vertebrae serve as a viable alternative source for bone autografts in veterinary surgery. The efficacy of A-PRF+ enhanced osseous regeneration in treated radial bone defects, but it remained inferior to rib and coccygeal autografts.

Keywords: Rib bone autograft, Coccygeal bone autograft, A–PRF+, Radial bone defects, Corticocancellous autograft.

Introduction

Bone is recognized as the second most frequently grafted tissue following blood transfusion (Haugen *et al*., 2019). Autogenous bone transplants are the gold standard for several reasons. Osteoblasts in osseous grafts promote osteogenesis under the influence of local cytokines. The cancellous bone matrix releases a multitude of cytokines and growth factors from the extracellular matrix (osteoinductive). A correctly harvested graft provides a framework for bone growth (osteoconduction) (Miron *et al*., 2011).

Autogenous bone grafts are classified as cortical, cancellous, corticocancellous grafts, and bone marrow components. The cortical bone can be further categorized into vascularized and nonvascularized types (Tang *et al*., 2021). Cortical bone autografts mainly demonstrate osteoconductive properties, with limited osteoinductive and osteogenic capabilities, while providing remarkable mechanical support. Numerous locations have been employed to harvest the cortical grafts, including the iliac crest, fibula, distal radius, and rib (Nashi and Kagda, 2023). Cancellous autografts possessing all requisite qualities demonstrate significant osteoconductive, osteoinductive, and osteogenic properties; yet, they are deficient in mechanical support. The iliac crest (anterior or posterior), distal radius, distal femoral metaphysis, or proximal tibia are the sources of cancellous bone grafts. Corticocancellous grafts provide the advantages of both cortical and cancellous

***Corresponding Author:** Taher Naser Elmeshreghi. Department of Surgery and Theriogenology, Faculty of Veterinary Medicine, University of Tripoli, Tripoli, Libya. Email: *elmeshreghi.taher@gmail.com*

bone transplants, rendering them a favored option. It is most frequently obtained from the iliac crest, fibula, ribs, or laminae when standard cervical, thoracic, or lumbar laminectomy (Jakoi *et al*., 2015; Migliorini *et al*., 2021).

The rib, which supplies bone and cartilage or both, is one of the most important sources of nonvascularized corticocancellous autografts. Rib bone grafts can be used to repair defects in the craniofacial region, limbs, or occipitocervical atlantoaxial and subaxial cervical spines (Sawin *et al*., 1998; Zhang *et al*., 2024). In a case series study of various osseous tissue defects in the craniofacial region, the rib graft was found to be a safe, well-accepted treatment with relatively low morbidity. It offers a significant quantity of dependable grafting materials, enabling the successful restoration of various head and neck region abnormalities (Al-khannaq *et al*., 2024).

In veterinary orthopedic surgery, nonvascularized autogenous corticocancellous coccygeal vertebral grafts are considered a promising choice. Limited research data exist; the only experimental study conducted aimed to address segmental defects in the ulna by using the tail vertebral bone alongside the iliac bone in dogs. The findings of this study emphasize that the tail vertebral bone is an outstanding source of bone graft material (Baniadam *et al*., 2006).

Platelet-rich fibrin (PRF) is the second-generation type of autologous platelet concentrate and biomaterial that was initially used in 2001 by Choukroun *et al*. (2001). Advanced platelet-rich fibrin plus (A-PRF+) derived through the application of the principles of low force and reduced time of centrifugation, the elevated release of growth factors in A-PRF+ can be attributed to a greater number of leukocytes trapped in the three-dimensional fibrin matrix (Shah *et al*., 2017). A-PRF+ showed a greater release of growth factors compared to leukocyte- and platelet-rich fibrin (L-PRF) and advanced platelet-rich fibrin (A-PRF). These growth factors include platelet-derived growth factor AB, transforming growth factor b-1, and vascular endothelial growth factor. It has been shown to enhance bone repair and stimulate cell proliferation and differentiation (Fujioka-Kobayashi *et al*., 2017; Kirilova *et al*., 2022; Kosmidis *et al*., 2023).

The treatment of segmental bone defects poses a significant challenge in human and veterinary medicine. The efficacy of autogenous corticocancellous bone grafts, such as those derived from the rib bone and coccygeal vertebrae, and autogenous platelet concentrates, such as A-PRF+, in the treatment of segmental bone defects has not been extensively studied. Therefore, the objectives of the current study were to ascertain the feasibility of using autogenous rib bone and coccygeal vertebrae transplants to treat and promote bone regeneration in rabbits with experimentally induced diaphyseal radial bone defects compared to A-PRF+.

Materials and Methods

Experimental animals and groups

The experimental study used 24 male white New Zealand rabbits, each of which weighed 2.5 ± 0.5 kg at 3 months of age. The animals were confined in separate, standard cages that were appropriately sized and maintained at a temperature of 25°C with a 12-hour light/dark cycle. Commercial rabbit food and water were provided *ad libitum*.

The rabbits were randomly assigned to four groups, each consisting of six rabbits. The induced radius mid-shaft segmental bone defects, measuring 10 mm in the left limb, were treated according to designated groups: the control group left the defects unfilled, the A-PRF+ group filled the defects with A-PRF+, the coccygeal group used the third coccygeal vertebra post-caudectomy to fill the defects, and the rib group used the 11th rib for filling the defects.

Preparation of the A–PRF+

To obtain A-PRF+, a total of 10 ml of blood was collected from the marginal ear vein of the rabbits in the A-PRF+ group in two sterile plain tubes without anticoagulant, as previously described by Fujioka-Kobayashi *et al*. (2017). The blood samples were centrifuged at 1,300 rpm for 8 minutes at room temperature to obtain the fibrin clot in the uppermost of the tubes. The fibrin clots were left for 15 minutes before their implantation in the defect site, as shown in Figure 1.

Harvesting of the coccygeal vertebrae

A partial caudectomy was performed to harvest the third coccygeal vertebra. A double V-shaped incision was made in the skin tissue distal to the intended site of the intervertebral transection. After dissection, the blood vessels of the tail at the ventral and medial aspects of the tail were ligated cranially to the site of transection using 2/0 vicryl (Egysorb, Obour City, Cairo, Egypt). The surgical incision was closed routinely with a 2/0 vicryl in a simple interrupted suture pattern. A tail bandage was performed for 1-week post-surgery. The surrounding soft tissues were carefully separated from the harvested vertebrae. The third coccygeal vertebra was implanted at the radial defect site.

Harvesting of the rib

The surgical technique for harvesting the 11th floating rib was conducted on the right lateral costal. Following clipping and shaving, the surgical field was aseptically cleansed and prepared. A 3 cm longitudinal incision over the 11th rib was made in the skin, subcutaneous tissue, and muscle to carefully expose the rib. Then, 2 cm of the rib was excised, the edge was reshaped, and the downside cartilaginous section was removed to yield a final 10 mm 11th floating rib ready for implantation. The operating incision was closed with 2/0 vicryl for the muscle and subcutaneous tissue and 2/0 braided silk sutures (EGYSILK, Taisier. Co-Med, Obour City, Egypt) for the skin.

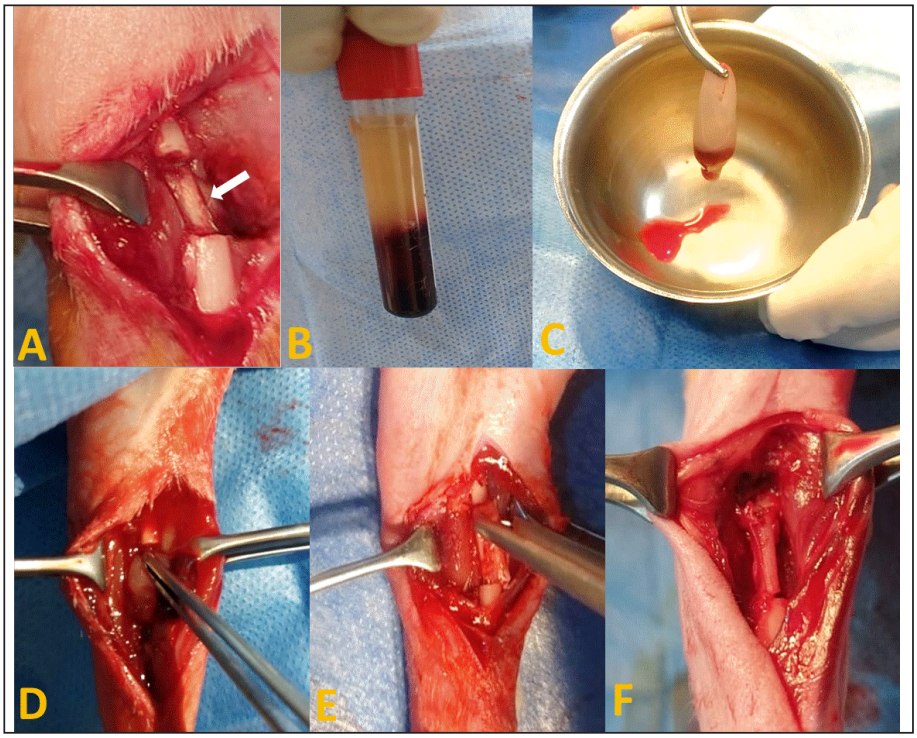

Fig. 1. Autogenous radius bone grafting in rabbits (A): Control group: the defect was left untreated. The white arrow indicates the ulnar bone. (B) and (C): Prepared fibrin clot of A-PRF+. (D): The defect was implanted in A-PRF+. (E) The defect was implanted with the third coccygeal vertebra. (F): The defect was implanted in the 11th rib.

Surgical procedure

The rabbits were pre-anesthetized with 0.75 mg/kg of intramuscularly administered acepromazine maleate 1.5% (Castran, Interchemie CO., Netherlands) and a subcutaneous injection of xylazine 2% (Xyla, Interchemie CO., Netherlands) at a dose of 5 mg/kg. The induction of general anesthesia was performed with 35 mg/kg of 5% ketamine hydrochloride (Panpharma Laboratory, Fougères, France) administered intramuscularly (Boudra *et al*., 2020). The left forelimbs of rabbits were prepared for surgery by shaving and aseptically preparing the skin with 10% povidone-iodine. The animals were then positioned laterally on the operating table. Under general anesthesia, a 4 cm craniomedial surgical incision was made across the left forelimb. The muscles were dissected to expose the radius. A 10 mm segmental radius bone defect was created at the diaphyseal site of the bone, and the interosseous ligament was surgically severed, facilitating the removal of the bone segment.

The treatment of radius bone defects was performed according to the designated group distribution, as shown in Figure 1. After filling the bone defect, the internal fixation of the radius was considered unnecessary because the ulna provided adequate support. The surgical incision was subsequently closed with 2/0 vicryl sutures for the muscle and subcutaneous layers and 2/0 braided silk sutures for the skin.

Cefazolin sodium 1 g (Zinol, Pharco Pharmaceuticals, Alexandria, Egypt) was given intramuscularly for 5 days at a dosage of 20 mg/kg (Demirel and Aksakal, 2015). To alleviate postoperative pain, meloxicam 0.75% (Amriya Pharmaceutical Industries, Alexandria, Egypt) was administered at a dosage of 0.6 mg/kg subcutaneously for a duration of 3 days (Varga, 2014). The rabbits were monitored in a recovery room post-surgery until they regained consciousness. The surgical skin stitches were taken out 7 to 10 days after the operation. The rabbits were sacrificed at 6 and 12 weeks following the surgery. Radiography and computed tomography (CT) were used to assess the treated radius bone defects, along with histopathological evaluation including macroscopic and microscopic analyses.

Radiography and CT scan

A radiographic evaluation was conducted using an X-ray generator (Pox-300 BT, Toshiba, RotanodeTM, Japan) with exposure factors of 2.5 mAs, 40 kVp, and 50 mA. A mediolateral radiograph was acquired on the day of surgery, as well as at 6 and 12 weeks post-surgery. Two orthopedic specialists independently assessed the treated bone defect area using the Lane–Sandhu radiographic scoring criteria, as shown in Table 1 (Zhao *et al*., 2021).

CT scans of repaired radius bone defects were performed at 6 and 12 weeks postoperatively using a GE Lightspeed VCT 64 CT system (WIPRO GE HEALTHCARE PVT. LTD., Karnataka, India) at 140 KV and 50 mA. The RadiAnt DICOM viewer (Medixant, Poznan, Poland) was used to visualize the reconstructed coronal and three-dimensional (3D) images. The treated bone defect site was scored by two blinded orthopedic experts using Cheung's grading standards, as shown in Table 2 (Ibrahim *et al*., 2016).

Histopathological evaluation

Evaluations at the macroscopic level were conducted 6 and 12 weeks post-surgery. The soft tissue was removed from the left radius and ulnar bone. The bones were subsequently imaged and assessed by two specialists using the scoring system of 0 to +3 as defined by Parizi *et al*. (2013). A score of 0 signifies complete instability at the defect site, indicating nonunion. Scores of +1 and +2 were given when cartilage, soft tissue, or cracks were observed within the defect, suggesting a potentially unstable union. Bone bridging, signifying a complete union, was assigned a score of +3.

Samples from repaired radius bone defects of rabbits were collected for microscopic examination at 6 and 12 weeks post-operations using a slow-speed saw. The samples were then fixed in a 10% buffered neutral formalin solution for 48 hours, decalcified for 3 weeks in a mixture of hydrochloric acid HCl 10% and formic acid 10%, dehydrated in an increasing ethanol gradient, cleared in xylene, and embedded in paraffin wax. Five micron-thick paraffin block sections were cut using a microtome (Leica RM 2155, England). The defect sites were subjected to longitudinal sections. Hematoxylin and eosin (H and E) and Masson's trichrome were used to stain the specimens. Two separate histopathologists conducted the assessment process blindly, examining and analyzing all slides from all groups using Emery's scoring system, as shown in Table 3 (Emery *et al*., 1994).

Statistical analysis

All quantitative diagnostic imaging and histopathological data collected were presented in the means and standard deviations. Statistical data analyses (one-way analysis of variance) were performed using GraphPad Prism version 10.3.0 (GraphPad Software, La Jolla, CA, United States). Statistical differences were identified between the groups, with significant results ($p < 0.05$) and highly significant results ($p < 0.01$ and $p < 0.001$).

Ethical approval

The current study protocol was approved and committed to the ethical regulations for the care

Table 1. Lane–Sandhu radiographic scoring criteria.

Category	Standard	Scores
Bone formation	No evidence of bone formation	0
	Bone formation occupying 25% of defect	1
	Bone formation occupying 50% of defect	2
	Bone formation occupying 75% of defect	3
	Full gap bone formation	4
Fracture line	Clear	0
	Relatively clear	1
	Partial fracture line	2
	Basically vanished	3
	Completely vanished	4
Bone remodeling	No evidence of remodeling	0
	Remodeling of medullary canal	2
	Full remodeling of cortex	4

Table 2. Cheung's grading standards.

Grade	Radiographic description
Grade 1	Indicates no calcification at the fracture site.
Grade 2	Indicates patchy calcification
Grade 3	Indicates that the calcification takes on the appearance of the callus
Grade 4	Shows callus bridging across the fracture gap
Grade 5	Indicates continuity of bone trabeculae
Grade 6	Demonstrates remodeling to normal bone

Table 3. Emery's scoring system.

Item	Score
Empty gap	0
Filled with fibrous connective tissue only	1
More fibrous tissue than fibrocartilage	2
More fibrocartilage than fibrous tissue	3
Fibrocartilage only	4
More fibrocartilage than bone	5
More bone than fibrocartilage	6
Filled only with bone	7

and use of laboratory animals in accordance with the guidelines of the Animal Welfare and Research Ethics Committee of Zagazig University, Egypt (ZU-IACUC/2/F/230/2024).

Results

The postoperative evaluation of radiological findings, as illustrated in Figure 2, revealed radiolucency in both the control and A-PRF+ groups. In the coccygeal and rib groups, the implanted third coccygeal vertebra and the rib bone filled the defect location with a radiopaque appearance. The fracture line was plainly visible in the X-ray images of the designated control group at 6 weeks and 12 weeks post-operation, as shown in Figure 2, with the rate of new bone formation being limited. The A-PRF+ group presented new bone formation at the fracture site at 6 weeks, and the fracture persisted to be visible. At 12 weeks, the rate of bone formation increased significantly, and the fracture line completely disappeared. The plain radiographs in the coccygeal and rib groups demonstrated a more visibly developed bone formation at 6 weeks. However, the fracture line only partially emerged. By 12 weeks, the bone had formed and the fracture site had completely bridged, indicating the end of the healing process.

The statistical outcomes from the Lane–Sandhu scores (Fig. 3) indicated that the rib group exhibited

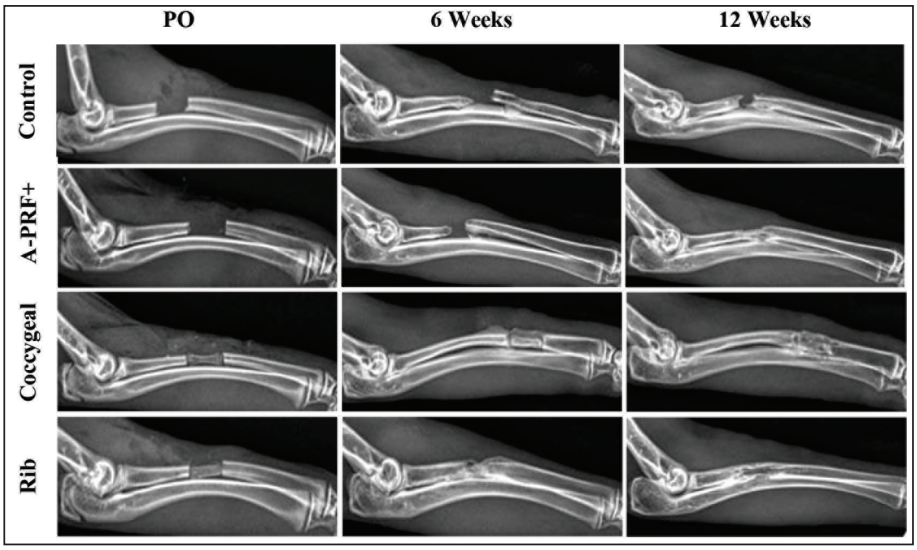

Fig. 2. Radiographic evaluation (mediolateral views) of surgically repaired segmental radius bone defects in rabbits. The radiographs illustrate the bone formation in the control, A-PRF+, coccygeal, and rib groups at postoperatively (PO), 6, and 12 weeks post-surgical intervention.

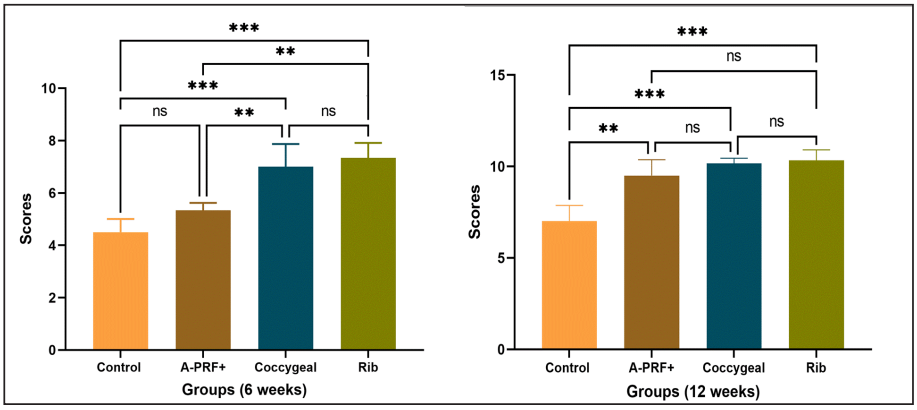

Fig. 3. The graphs illustrate Lane–Sandhu radiographic scoring results at 6 and 12 weeks postoperatively. The findings were displayed as the mean and standard deviation for each group. The symbols ** and *** indicated statistically significant differences, corresponding to *p* values of less than 0.01 and 0.001, respectively. The symbol ns signified that there was no statistically significant difference present.

a higher bone formation score, while the coccygeal group followed at 6 weeks postoperatively. Significant differences were observed in the rib and coccygeal groups compared to the control ($p < 0.001$) and A-PRF+ ($p < 0.01$) groups. By the 12 week post-implantation, the treated A-PRF+, coccygeal, and rib groups achieved a significantly higher rate of bone formation compared to the control group ($p < 0.01$), ($p < 0.001$), and ($p < 0.001$), respectively.

The results of the CT examination for untreated and repaired bone defects are presented as a three-dimensional reconstructed image in Figure 4. The untreated control group confirmed a lack of bone formation, showing a clear bone gap at both the 6- and 12-week time points. The bone gap continued to be noticeable in the treated A-PRF+ group at 6 weeks, despite an increase in bone tissue growth. In the coccygeal and rib groups, bone tissue growth was guided by bridging the gap without entirely closing it at 6 weeks. In the A-PRF+, coccygeal, and rib groups, the newly formed bone was fully integrated with the adjacent host bone at 12 weeks' post-implantation.

The graphs in Figure 5 reflect the results of Cheung's CT score. The rib group had significantly higher grades than the control and A-PRF+ groups at 6 weeks post-implantation. The data revealed statistical significance between the rib and control group ($p < 0.01$), the rib and A-PRF+ group ($p < 0.05$), and the coccygeal and control group ($p < 0.05$). The A-PRF+ scores were not statistically different from those of the control group ($p > 0.05$). Cheung's CT scoring revealed a significant difference between the rib, coccygeal, and A-PRF+ groups and the control group at 12 weeks, with p values less than 0.01 and 0.05, respectively, but no statistical significance was seen between groups.

As shown in Figure 6, the macroscopic analysis of the bone specimens confirmed the presence of soft tissue within the defects as well as the absence of fusion with the host bone. The defects were clearly observed in the control group at both 6 and 12 weeks' post-implantation, as well as in the A-PRF+ group at 6 weeks. In the rib

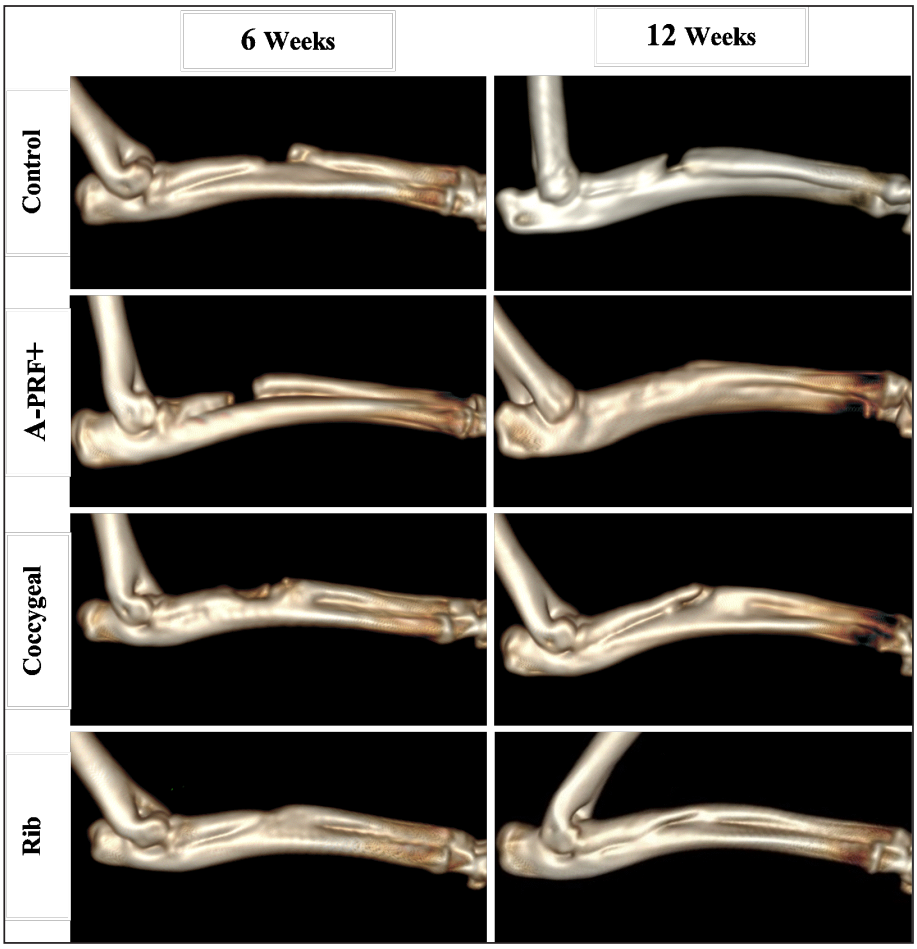

Fig. 4. Three-dimensional CT scans were utilized to assess bone formation for the control, A-PRF+, coccygeal, and rib groups of rabbits with treated segmental bone defects at 6 and 12 weeks post-surgery.

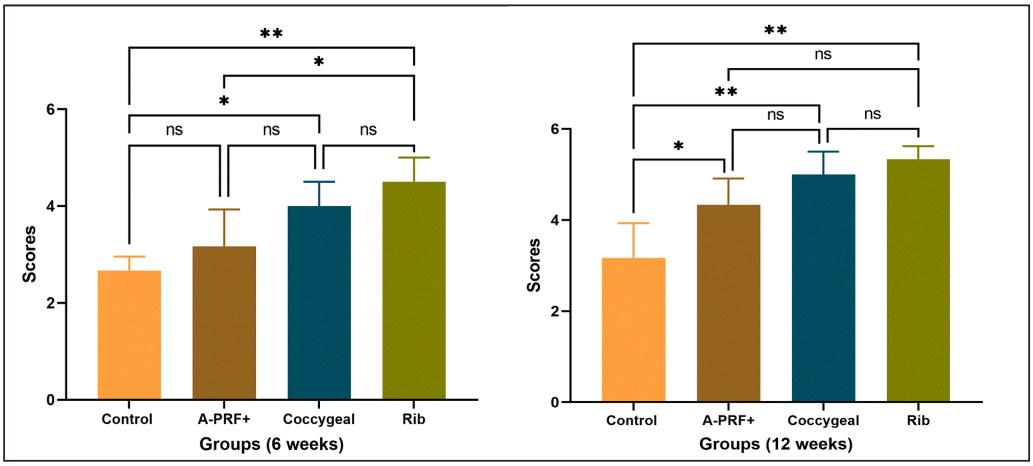

Fig. 5. The graphs illustrate Cheung's CT scoring results at 6 and 12 weeks postoperatively. The findings were displayed as the mean and standard deviation for each group. The symbols * and ** indicated statistically significant differences, corresponding to *p* values of less than 0.05 and 0.01, respectively. The symbol ns signified that there was no statistically significant difference present.

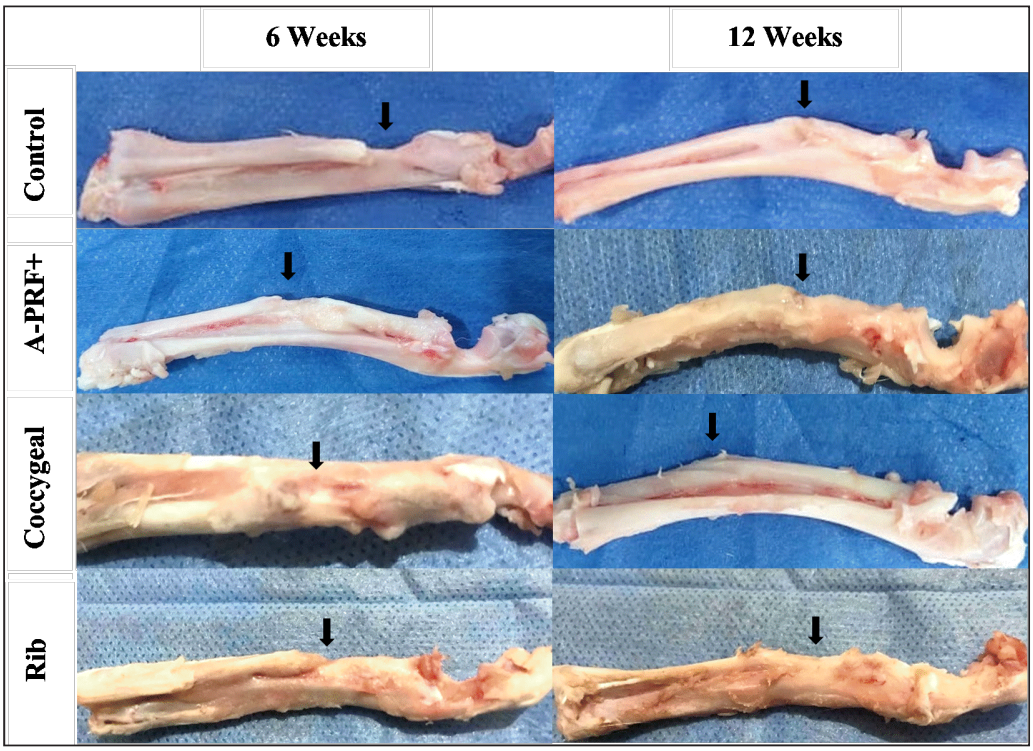

Fig. 6. Macroscopic images of treated radius bone defects across four groups at two time intervals (6 and 12 weeks) post-implantation, with the black arrow highlighting the area of interest.

and coccygeal groups, partial bone fusion with the host bone was observed 6 weeks after surgery. In contrast, at 12 weeks of treatment, the A-PRF+, coccygeal, and rib groups had completely healed their bones since the defect had been replaced with hard tissues that were identical to bone.

The macroscopic image scoring results of bone specimens, as shown in Figure 7, indicated that the rib groups scored significantly higher than the untreated control group ($p < 0.01$) and the coccygeal group scored significantly higher than the control group ($p < 0.05$) at 6 weeks post-surgical treatment. At the

same time, no statistically significant differences were observed between the other groups. At 12 weeks' post-implantation, the A-PRF+, coccygeal, and rib groups demonstrated statistically significant differences as compared to the control group ($p < 0.05$).

Histopathological sections in Figure 8, stained with H and E, found that the bone defect was substituted by more fibrous connective tissue and a reduced presence of calcified cartilaginous tissue and newly formed bone at 6 and 12 weeks post-implantation. At 6 weeks, the A-PRF+ group repaired defect sites with centrally placed hyaline cartilage and fewer calcified chondrocytes. In the coccygeal-treated group at 6 weeks, the bone gap was occupied by newly hyaline cartilage close to the trabecular bone newly formed, with obvious calcified chondrocytes and intervening marrow cavities. The rib group defect location contained mature lamellar bony structures and equivalent amounts of calcified cartilaginous tissue with wide marrow gaps, as well as peripherally distributed granulation tissue at 6 weeks post-operatively. Histopathological sections of the A-PRF+, coccygeal, and rib groups exhibited lamellar bone dominant with lees calcified cartilaginous tissue at 12 weeks.

Masson's trichrome-stained sections in Figure 9 of the control group showed hypercellular fibrous connective tissue alongside fewer neo-fibrocartilages and osseous tissues. The A-PRF+ group had a greater central cartilaginous mass and a few peripheral immature and mature bone tissue at 6 weeks. At 6 weeks, chondroblastic ossification with activated osteoblasts was observed in the coccygeal group. The hyaline matrix and slightly stained mature bone matrix were also present. The 6-week rib group consisted of a mixture of mature and immature bone and cartilage. The osteoblast-surrounded fibrous tissue core was also included. Mature lamellar bone tissue was prevalent in the A-PRF+, coccygeal, and rib groups at 12 weeks after implantation.

Emery's histological score varied significantly between the rib and control groups, as well as the coccygeal and control groups, at 6 weeks' post-surgery ($p < 0.05$). However, none of these variations were observed in the other groups (Fig. 10). At 12 weeks postoperatively, the A-PRF+ coccygeal group showed statistical significance compared with the control group ($p < 0.05$) and compared with the rib and control group ($p < 0.01$), as shown in Figure 10.

Discussion

In orthopedic surgery, the management of segmental bone defects remains challenging. This study assessed the regeneration efficiency of several autologous rib and coccygeal bones, as well as autologous A-PRF+, for the treatment of segmental defects created in rabbit radial bone.

The present study demonstrated that the rib group achieved the maximum bone healing score at 6 and 12 weeks postoperatively, with a statistically significant difference between the rib group and the control group in all diagnostic imaging and histopathological analyses. According to the author's knowledge, limited research has been available on the use of rib bone grafting for the repair of segmental defects in long bones. In accordance with our study, a cat with femoral nonunion underwent treatment involving a combination of free nonvascularized autogenous rib and iliac bone in addition to rhBMP-2. Bone healing commenced 2 months' post-surgery and continued for a duration of 1 year. Despite the ongoing moderate lameness, the cat's ability to move and overall quality of life remained satisfactory (Chung *et al*., 2021). In

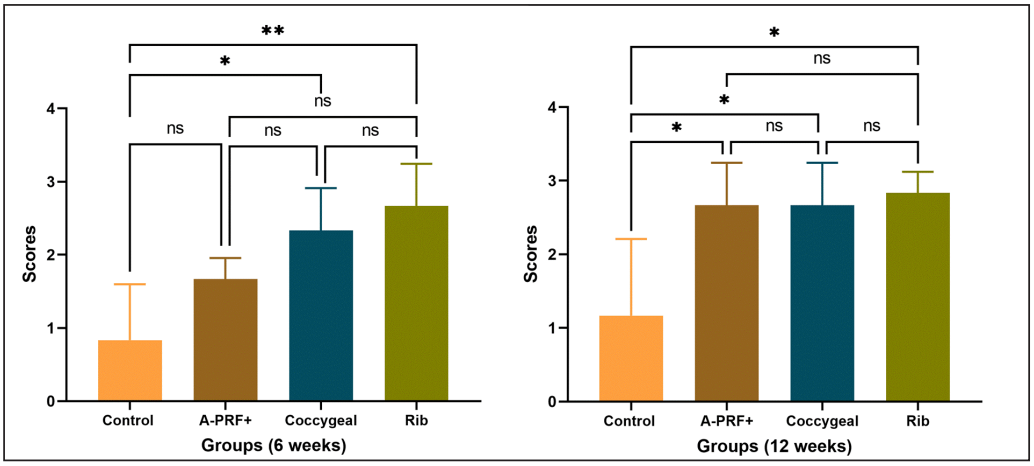

Fig. 7. The graphs illustrate macroscopic scoring results at 6 and 12 weeks postoperatively. The findings were displayed as the mean and standard deviation for each group. The symbols * and ** indicated statistically significant differences, corresponding to *p* values of less than 0.05 and 0.01, respectively. The symbol ns signified that there was no statistically significant difference present.

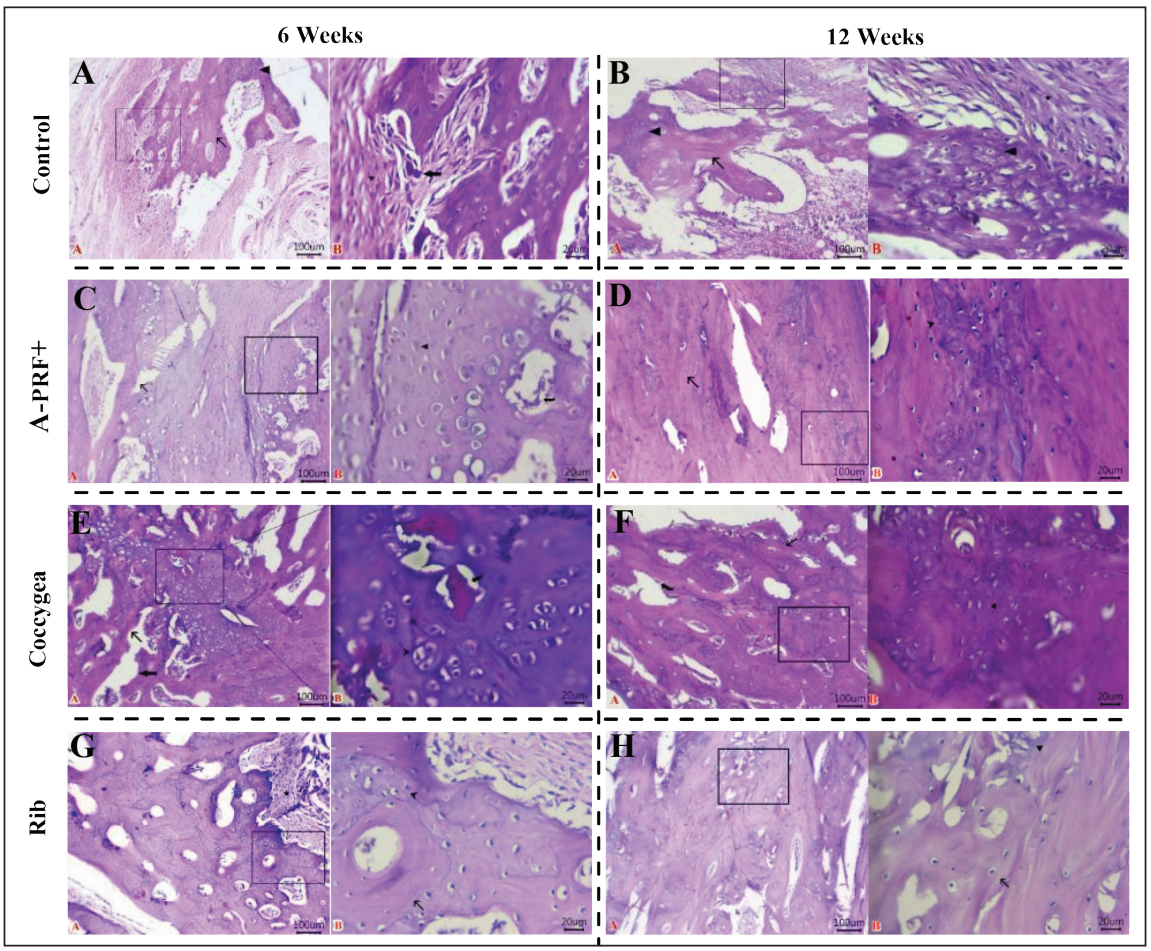

Fig. 8. Histopathological sections of repaired segmental defects in rabbits at 6 and 12 weeks post-surgical operation were stained with H and E. All photomicrographs were taken at a scale bar of 100 µm and a high magnification of 20 µm. (A): Fibrous connective tissue (stars), calcified cartilaginous masses (arrowhead), newly formed bony tissue (arrow), and osteoclasts (thick arrow) adhered to neoformed bone tissue. (B): Granulation tissue (star), trabecular bone tissue (arrow) with calcified cartilaginous tissue (arrowheads), and wide marrow spaces and osteoblastic activity. (C): Newly formed woven bones (arrow), fibrocartilaginous areas (red arrowhead), fibroplasia with excess collagen (star), and calcified chondrocytes (black arrowhead) lined along their periphery by active osteoblasts (curved arrow). (D): Maturation and remodeling of newly formed Haversian system (arrow) with prominent Haversian canals, marrow cavity, and few calcified cartilaginous tissues (arrowhead) within defect sites. (E): Newly formed hyaline cartilage (arrowhead), newly formed trabecular bones (arrow), calcified chondrocytes, and intervening marrow cavity (thick arrow). (F): Calcified matrix of some chondrocytes beside lamellar bony tissues in between (curved arrow). (G): Mature lamellar bone structures (arrow), equal quantities of calcified cartilaginous tissue (arrowhead) beside wide marrow spaces, and peripherally located granulation tissue (star). (H): Large area of matured bone tissue (arrow), marrow spaces with active osteoblast beside a few calcified cartilaginous tissues (arrowhead).

human surgery, rib bone grafts provide a source of free, nonvascularized corticocancellous material for the management of various head and neck deformities (Abdel-Haleem *et al*., 2011). Craniocervical junction abnormalities in children were successfully addressed using an autogenous rib bone graft, with bone fusion verified by CT imaging between 3 and 6 months postoperatively. None of the patients experienced postsurgical problems (Deng *et al*., 2024). The rib bone, serving as an autologous corticocancellous graft, stands out as an excellent option due to its combination of the reliable structural integrity of cortical bone, which offers mechanical support, and cancellous bone, which is abundant in osteoblasts and osteocytes, thereby boosting its osteogenic potential. Our findings established beyond a reasonable doubt that transplanted rib bone promotes bone formation in radial bone defects, despite the fact that mechanical characteristics were not measured. Sharifi *et al*. (2012) provided proof regarding the biomechanical properties of rib bone

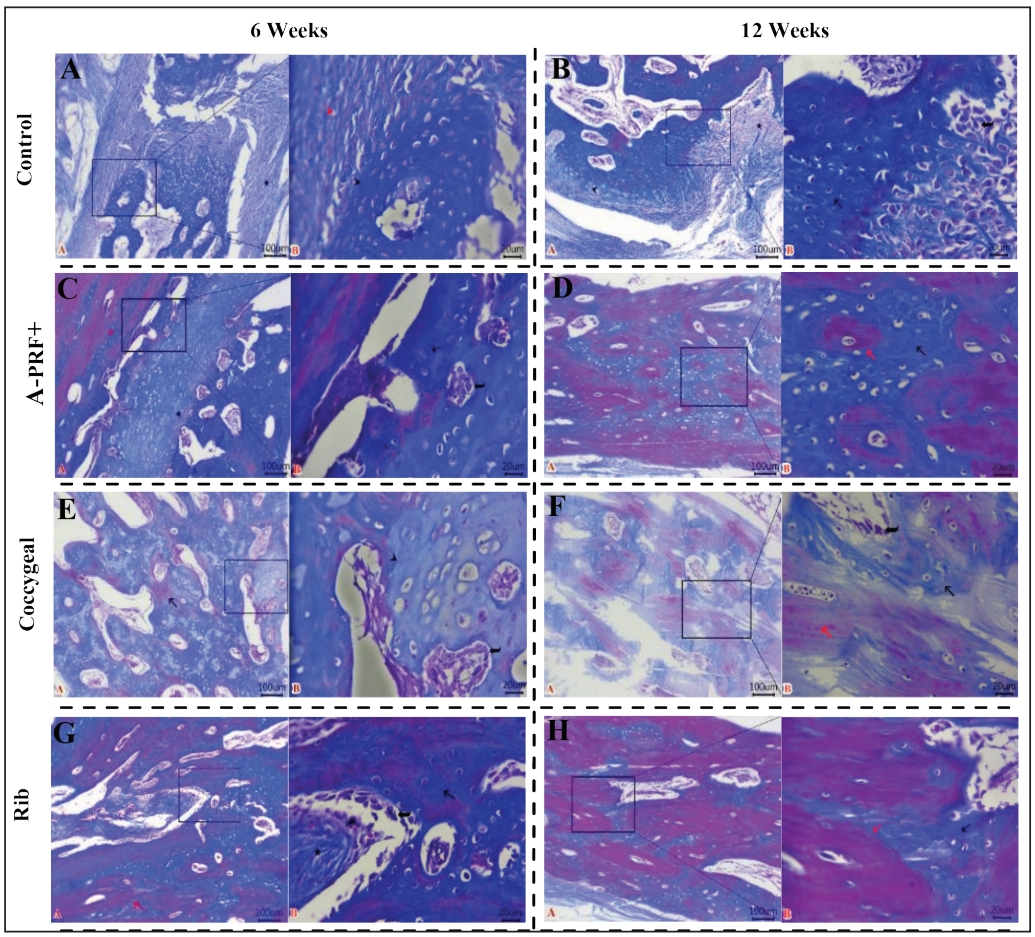

Fig. 9. Histopathological sections of repaired segmental defects in rabbits at 6 and 12 weeks post-surgical operation were stained with Masson's trichrome. All photomicrographs were taken at a scale bar of 100 µm and high magnification of 20 µm. **(A):** Fibrocartilaginous mass (red arrowhead), calcified chondrocytes (black arrowhead), and cellular fibrous tissue (star). (B): Hypercellular fibrous connective tissue (star), neo-fibrocartilage (black arrowhead), and neo-osseous tissue (arrow) active osteoblast (curved arrow). (C): Cartilaginous mass (arrowhead), immature bony tissue (arrow), mature bony tissue (red arrow), and activate osteoblasts within marrow cavity (curved arrow). (D): Mature osseous tissue (red arrow) was intermixed with less immature osseous tissue (black arrow). (E): Chondroblastic ossification with activated osteoblasts (curved arrow), hyaline matrix in newly formed cartilage (arrowhead), and mature bone matrix (arrow). (F): Lamellar bone tissue (red arrow) and immature bone tissue (black arrow) with active osteoblast cells (curved arrow) within the marrow cavity. (G): Mature bone tissue (red arrow), immature bony and cartilage tissues (black arrow), and core of fibrous tissue (star) encircled by osteoblast cells (curved arrow). (H): Mature osseous tissue (red arrow), immature osseous tissue (black arrow) beside large marrow spaces filled with osteoblasts.

by evaluating the impact of implanted autogenous rib bone, with or without nano-hydroxyapatite, on segmental defects induced in the radial bone of rabbits. Findings showed that autologous rib bone grafts, either alone or in combination with nano-hydroxyapatite, improved osseointegration while retaining strength and stiffness.

Coccygeal bones offer an alternative source of autogenous, nonvascularized bone transplantation for veterinary surgery. In the present work, the repair of radial-induced bone defects in rabbits using autogenous coccygeal bone showed outstanding partial bone healing at 6 weeks and complete bone union at 12 weeks. At 6 and 12 weeks post-surgery, X-ray, CT, and histological examinations showed a statistically significant difference between the coccygeal and control groups. In literature, limited case studies employing coccygeal bone autografts supplemented with either a cancellous graft collected from the humerus or biphasic calcium phosphate, platelet-rich plasma, and

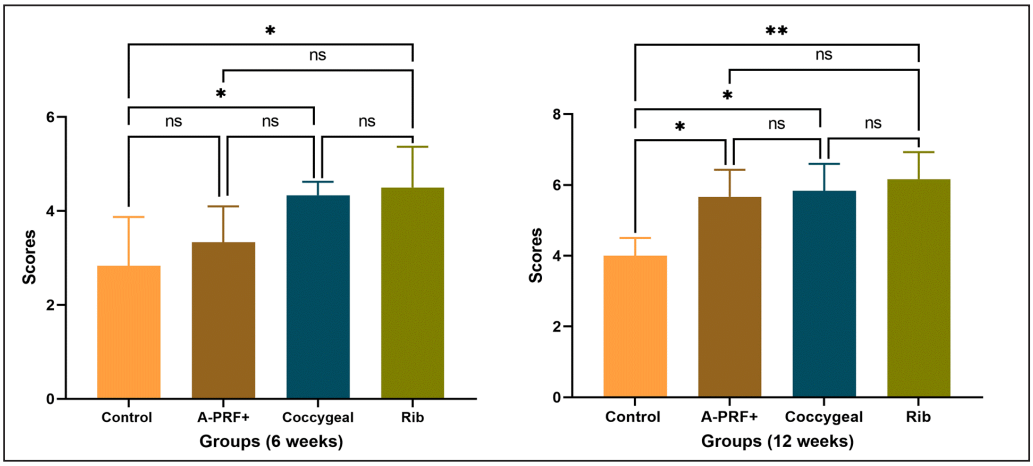

Fig. 10. The graphs illustrate Emery's histopathological scoring results at 6 and 12 weeks postoperatively. The findings were displayed as the mean and standard deviation for each group. The symbols * and ** indicated statistically significant differences, corresponding to p values of less than 0.05 and 0.01, respectively. The symbol ns signified that there was no statistically significant difference present.

bone morphogenetic proteins were applied to address defects in nonunion fractures of radioulnar and femoral bones in canines (Palumbo Piccionello *et al*., 2017; Choi and Yoon, 2022; Goto and Ikeda, 2022; Cho *et al*., 2023). Conversely, the coccygeal bone was implanted in the current experiment without the inclusion of an additional bone graft source. Our results align with previously cited case studies demonstrating successful bone regeneration and the viability of using coccygeal vertebral bone for addressing long bone defects.

Many standout features make using coccygeal bone vertebrae to treat segmental bone defects an excellent option. Corticospongious coccygeal bone grafts offer advantages because of their osteogenic properties and structural support. *In vitro* study examined equine cancellous bones from different donor sites for osteogenicity. The fourth coccygeal vertebra offers good osteogenic potential (McDuffee and Anderson, 2003). *Ex vivo* study in canines examined the biomechanical and morphological characteristics of coccygeal vertebrae as an alternative to conventional bone autografts. The coccygeal vertebrae had considerable compressive strength, with the content of cancellous bone in the ilium wing, coccygeal, and rib bones recorded at 69%, 42%, and 26%, respectively (Serafini *et al*., 2018). Additionally, researchers found that the coccygeal vertebral bone diameter in dogs was compatible and potentially well-suited with the radial bone defect site (Serafini *et al*., 2018; Choi and Yoon, 2022). This was consistent with the method outlined in our experimental study, which demonstrated that the third vertebral coccygeal bone was ideally suited for implantation in rabbits with induced radial bone defects.

A-PRF+ is an autologous, blood-derived bioactive substance with a porous fibrin matrix that is endogenously loaded with growth factors, leukocytes, and platelets. It is easy to prepare, and it is immune-negative. The conventional solid form of PRF was created by increasing the rotational centrifugal force (RCF). This resulted in a decrease in cell quantity and negatively impacted the secretion of growth factors (Choukroun and Ghanaati, 2018; Ozer *et al*., 2019). Consequently, A-PRF was produced using the low-speed centrifugation concept, showing improved entrapment of B- and T-lymphocytes along with a more uniform distribution of platelets and neutrophils. The quantity of viable cells, including platelets, was significantly greater in A-PRF within the distal region of the fibrin clots. A-PRF+ was the final solid form of PRF obtained by lowering RCF and time. As a result, a greater number of cells can be collected within the upper layer of the fibrin clot (Shah *et al*., 2017).

The findings of our experimental study revealed statistically significant differences at 12 weeks postoperatively between the A-PRF+ and control groups across all quantitative measurement methods of evaluation. In terms of enhanced bone formation, the results of our study are consistent with those that have been successfully used as regenerative periodontal therapy in a variety of periodontal surgical procedures. In addition to addressing intrabony defects, these procedures involve the treatment of chronic apical periodontitis, socket preservation, and ridge augmentation (Csifó-Nagy *et al*., 2021; Yewale *et al*., 2021; Kirilova *et al*., 2022; Machut and Żółtowska, 2022; Lahham *et al*., 2023). This study is the first to assess A-PRF+ as a potential treatment for segmental bone defects in the radius of rabbits. To our knowledge, no published research has examined the efficacy of A-PRF+ as a sole material for inducing bone regeneration in segmental bone

defects. Conversely, both traditional PRF and A-PRF were evaluated individually and in conjunction with a variety of supplemental bone graft materials. According to the study findings, the osteogenic and osteoinductive characteristics of PRF and A-PRF are responsible for their repairing properties. Enhanced bone healing was observed when osteoconductive bone graft materials were concurrently used (Wong *et al*., 2021; Zalama *et al*., 2022; Abd-Elkawi *et al*., 2023). The present study illustrated that the regenerative effects of A-PRF+ are attributable to a greater concentration of leukocytes within fibrin clots, which is correlated with an increase in growth factor release. The heightened cellularity of A-PRF+ is associated with an increase in macrophages, which play a crucial role in achieving a 23-fold enhancement in osteoblast differentiation (Chang *et al*., 2008). A-PRF+ released considerably more total growth factors than A-PRF and L-PRF. It plays a pivotal role in bone healing because of its strong angiogenic capabilities and ability to stimulate osteogenic differentiation and proliferation, thereby enabling the formation of new bone (Fujioka-Kobayashi *et al*., 2017; Basal *et al*., 2018; Wang *et al*., 2023; Nair *et al*., 2024).

Conclusion

This study experimentally examined the regeneration capacity and utility of various autogenous grafting materials for repairing full-thickness diaphyseal segmental defects in rabbit radial bone. Quantitative assessment using diagnostic imaging and histological methods confirmed the effectiveness of autogenous corticospongious rib and coccygeal bone implants and enhanced bone repair. An alternative source of coccygeal bone has shown promise for veterinary surgery. Based on the same evaluation methodologies, A-PRF+ showed osteoinductive healing properties for repairing radial bone lesions but with lower healing capacity than autogenous rib and coccygeal bone grafts.

Acknowledgments

The authors thank the staff members of the Surgery Department, Faculty of Veterinary Medicine, Zagazig University, Egypt, for their cooperation and support.

Conflict of interest

The authors declare no conflicts of interest.

Funding

None.

Authors' contributions

Experimental methodology: F.D.E., M.G., S.A.E., M.A., and T.N.E. Surgical procedures: T.N.E. and M.A. Surgical intervention supervision: F.D.E., M.G., and S.A.E. Postoperative care: T.N.E. Data acquisition and management T.N.E. and M.A. performed an analysis and interpretation of the data and composed the initial manuscript draft. T.N.E. Supervision F.D.E. All authors have evaluated and approved the completed version of the manuscript.

Data availability

All data related to the study findings are included in the manuscript.

References

Abd-Elkawi, M., Sharshar, A., Misk, T., Elgohary, I. and Gadallah, S. 2023. Effect of calcium carbonate nanoparticles, silver nanoparticles and advanced platelet-rich fibrin for enhancing bone healing in a rabbit model. Sci. Rep. 13(1), 15232.

Abdel-Haleem, A.K., Nouby, R. and Taghian, M. 2011. The use of the rib grafts in head and neck reconstruction. Egypt. J. Ear Nose Throat Allied Sci. 12(2), 89–98.

Al-khannaq, Y.R., Altimmimi, H.M. and Aubed, A.S. 2024. The use of autogenous rib graft in craniofacial reconstruction: case series study. Al-Rafidain J. Med. Sci. 7(1), 203–208.

Baniadam, A., Saberi Afshar, F., Ghadiri, A.R. and Karimi Jalalabadi, Z. 2006. The use of tail vertebra as cortical bone graft in experimentally induced ulnar defects in dogs. Iran. J. Vet. Surg. 01(1), 22–30.

Basal, O., Atay, T., Ciris, İ.M. and Baykal, Y.B. 2018. Epidermal growth factor (EGF) promotes bone healing in surgically induced osteonecrosis of the femoral head (ONFH). Bosn. J. Basic Med. Sci. 18(4), 352–360.

Boudra, A., Benbelkacem, I., Merati, R., Achour, H. and Daouadji, I. D. 2020. Comparison between three fixed anaesthesia protocols in rabbits. J. Prev. Vet. Med. 44(3), 99–103.

Chang, M.K., Raggatt, L.J., Alexander, K.A., Kuliwaba, J.S., Fazzalari, N.L., Schroder, K., Maylin, E.R., Ripoll, V.M., Hume, D.A. and Pettit, A.R. 2008. Osteal tissue macrophages are intercalated throughout human and mouse bone lining tissues and regulate osteoblast function *in vitro* and *in vivo*. J. Immunol. 181(2), 1232–1244.

Cho, K., Lee, K., Kang, K. and Kim, M. 2023. Treatment of a large defect induced by atrophic nonunion of femoral fracture in a dog with autogenous coccygeal bone grafting. Vet. Sci. 10(6), 388.

Choi, J.Y. and Yoon, H.Y. 2022. Use of coccygeal vertebra autograft and platelet-rich plasma for treating a distal radial nonunion fracture in a small-breed dog. Can. Vet. J. 63(7), 689–694.

Choukroun, J., Adda, F., Schoeffler, C. and Vervelle, A. 2001. Une opportunité en paro-implantologie: le PRF. Implantodontie 42(55), e62.

Choukroun, J. and Ghanaati, S. 2018. Reduction of relative centrifugation force within injectable platelet-rich-fibrin (PRF) concentrates advances patients' own inflammatory cells, platelets and growth factors: the first introduction to the low speed centrifugation concept. Eur. J. Trauma Emerg. Surg. 44(1), 87–95.

Chung, C.S., Lin, L.S. and Teo, Y.M. 2021. Case report: treatment of femoral non-union with rib and iliac crest autografts and rhBMP-2 in a cat. Front. Vet. Sci. 8, 756167.

Csifó-Nagy, B.K., Sólyom, E., Bognár, V.L., Nevelits, A. and Dőri, F. 2021. Efficacy of a new-generation platelet-rich fibrin in the treatment of periodontal intrabony defects: a randomized clinical trial. BMC Oral Health 21, 1–10.

Demirel, M. and Aksakal, B. 2015. Enhanced bone regeneration in rabbit tibial defects implanted with newly fabricated bioceramic bone grafts. Int. J. Appl. Ceram. 12(2), 254–263.

Deng, C., Zou, X., Yang, H., Fu, S., Chen, J., Ma, R., Xia, H. and Ma, X. 2024. Autologous rib grafts for craniocervical junction surgery in children: a clinical application. BMC Musculoskelet. Disord. 25(1), 494.

Emery, S.E., Brazinski, M.S., Koka, A., Bensusan, J.S. and Stevenson, S. 1994. The biological and biomechanical effects of irradiation on anterior spinal bone grafts in a canine model. J. Bone Joint Surg. 76(4), 540–548.

Fujioka-Kobayashi, M., Miron, R.J., Hernandez, M., Kandalam, U., Zhang, Y. and Choukroun, J. 2017. Optimized platelet-rich fibrin with the low-speed concept: growth factor release, biocompatibility, and cellular response. J. Periodontol. 88(1), 112–121.

Goto, M. and Ikeda, H. 2022. Use of an autologous bone graft derived from three caudal vertebrae for reconstruction in a dog with radioulnar atrophic nonunion and osteomyelitis. VCOT Open 05(02), e93–e97.

Haugen, H.J., Lyngstadaas, S.P., Rossi, F. and Perale, G. 2019. Bone grafts: which is the ideal biomaterial? J. Clin. Periodontol. 46, 92–102.

Ibrahim, M.R.M., Singh, S., Merican, A.M., Raghavendran, H.R.B., Murali, M.R., Naveen, S.V. and Kamarul, T. 2016. The effect of strontium ranelate on the healing of a fractured ulna with bone gap in rabbit. BMC Vet. Res. 12(1), 1–9.

Jakoi, A.M., Iorio, J.A. and Cahill, P.J. 2015. Autologous bone graft harvesting: a review of grafts and surgical techniques. Musculoskelet. Surg. 99(3), 171–178.

Kirilova, J., Kirov, D., Yovchev, D., Topalova-Pirinska, S. and Deliverska, E. 2022. Endodontic and surgical treatment of chronic apical periodontitis: a randomized clinical study. Biotechnol. Biotechnol. Equip. 36(1), 737–744.

Kosmidis, K., Ehsan, K., Pitzurra, L., Loos, B. and Jansen, I. 2023. An *in vitro* study into three different PRF preparations for osteogenesis potential. J. Periodontal Res. 58(3), 483–492.

Lahham, C., Ta'a, M.A., Lahham, E., Michael, S. and Zarif, W. 2023. The effect of recurrent application of concentrated platelet-rich fibrin inside the extraction socket on the hard and soft tissues. a randomized controlled trial. BMC Oral Health. 23(1), 677.

Machut, K. and Żółtowska, A. 2022. Plasma rich in growth factors in the treatment of endodontic periapical lesions in adult patients: 3-dimensional analysis using cone-beam computed tomography on the outcomes of non-Surgical endodontic treatment using A-PRF+ and calcium hydroxide: a retrospective cohort study. J. Clin. Med. 11(20), 6092.

McDuffee, L.A. and Anderson, G.I. 2003. *In vitro* comparison of equine cancellous bone graft donor sites and tibial periosteum as sources of viable osteoprogenitors. Vet. Surg. 32(5), 455–463.

Migliorini, F., Cuozzo, F., Torsiello, E., Spiezia, F., Oliva, F. and Maffulli, N. 2021. Autologous bone grafting in trauma and orthopaedic surgery: an evidence-based narrative review. J. Clin. Med. 10(19), 4347.

Miron, R., Hedbom, E., Saulacic, N., Zhang, Y., Sculean, A., Bosshardt, D. and Buser, D. 2011. Osteogenic potential of autogenous bone grafts harvested with four different surgical techniques. J. Dent. Res. 90(12), 1428–1433.

Nair, M.R., Thomas, R., Shah, R., Gowda, I. and Gowda, T.M. 2024. Comparison of the angiogenic efficacy of conventional leukocyte- and platelet-rich fibrin versus low-speed advanced platelet-rich fibrin: an *in vitro* chorioallantoic membrane assay study. Dent. Med. Probl. 61(1), 77–83.

Nashi, N. and Kagda, F.H.Y. 2023. Current concepts of bone grafting in trauma surgery. J. Clin. Orthop. Trauma. 43, 102231.

Ozer, K., Kankaya, Y., Colak, O. and Kocer, U. 2019 The impact of duration and force of centrifugation on platelet content and mass in the preparation of platelet-rich plasma. Aesthetic Plast. Surg. 43(4), 1078–1084.

Palumbo Piccionello, A., Salvaggio, A. and Volta, A. 2017. Caudal vertebra transfer: treatment of radio-ulnar nonunion and severe bone shortening in a dog. J. Small Anim. Pract. 58(1), 56–56.

Parizi, A.M., Oryan, A., Shafiei-Sarvestani, Z. and Bigham-Sadegh, A. 2013. Effectiveness of synthetic hydroxyapatite versus Persian Gulf coral in an animal model of long bone defect reconstruction. J. Orthop. Traumatol. 14(4), 259–268.

Sawin, P.D., Traynelis, V.C. and Menezes, A.H. 1998. A comparative analysis of fusion rates and donor-site morbidity for autogeneic rib and iliac crest bone grafts in posterior cervical fusions. J. Neurosurg. 88(2), 255–265.

Serafini, G.M.C., Pippi, N.L., Libardoni, R.D.N., Libardoni, R.d.N., Müller, D.C.d.M., Amaral, B.P., Zanella, I.G. and Cauduro, C.R. 2018. Coccygeal vertebra as an alternative to traditional autograft bone - tomography and biomechanical study in *ex vivo* dogs. Braz. J. Vet. 39(1), 54–60.

Shah, R., Triveni, M.G., Thomas, R. and Mehta, D.S. 2017. An update on the protocols and biologic actions of platelet rich fibrin in dentistry. Eur. J. Prosthodont. Restor. Dent. 25(2), 64–72.

Sharifi, D., Khoushkerdar, H.R., Abedi, G., Asghari, A. and Hesaraki, S. 2012. Mechanical properties of radial bone defects treated with autogenous graft covered with hydroxyapatite in rabbit. Acta Cir. Bras. 27(3), 256–259.

Tang, G., Liu, Z., Liu, Y., Yu, J., Wang, X., Tan, Z. and Ye, X. 2021. Recent trends in the development of bone regenerative biomaterials. Front. Cell Dev. Biol. 9, 665813.

Varga, M. 2014. Therapeutics. Textbook of rabbit medicine, 2nd ed. Butterworth, Malaysia: Heinemann, pp: 137–177.

Wang, F., Ye, Y., Zhang, Z., Teng, W., Sun, H., Chai, X., Zhou, X., Chen, J., Mou, H., Eloy, Y., Jin, X., Chen, L., Shao, Z., Wu, Y., Shen, Y., Liu, A., Lin, P., Wang, J., Yu, X. and Ye, Z. 2023. PDGFR in PDGF-BB/PDGFR signaling pathway does orchestrates osteogenesis in a temporal manner. Research 6, 0086.

Wong, C.C., Yeh, Y.Y., Chen, C.H., Manga, Y.B., Jheng, P.R., Lu, C.X. and Chuang, E.Y. 2021. Effectiveness of treating segmental bone defects with a synergistic co-delivery approach with platelet-rich fibrin and tricalcium phosphate. Mater. Sci. and Eng. C. 129, 112364.

Yewale, M., Bhat, S., Kamath, A., Tamrakar, A., Patil, V. and Algal, A.S. 2021. Advanced platelet-rich fibrin plus and osseous bone graft for socket preservation and ridge augmentation–a randomized control clinical trial. J. Oral Biol. Craniofacial Res. 11(2), 225–233.

Zalama, E., Karrouf, G., Rizk, A., Salama, B. and Samy, A. 2022. Does zinc oxide nanoparticles potentiate the regenerative effect of platelet-rich fibrin in healing of critical bone defect in rabbits? BMC Vet. Res. 18(1), 130.

Zhang, J., Li, S., He, H., Han, L., Zhang, S., Yang, L., Han, W., Wang, X., Gao, J., Zhao, J., Shi, W., Wu, Z., Wang, H., Zhang, Z., Zhang, L., Chen, W., Zhu, Q., Sun, T., Tang, P. and Zhang, Y. 2024. Clinical guidelines for indications, techniques, and complications of autogenous bone grafting. Chin. Med. J. 137(1), 5–7.

Zhao, L., Zhao, J., Tuo, Z. and Ren, G. 2021. Repair of long bone defects of large size using a tissue-engineered periosteum in a rabbit model. J. Mater. Sci. Mater. Med. 32(9), 105.